Inorganic Chemistry

Article

pubs.acs.org/IC

An Interconverting Family of Coordination Cages and a *meso*-Helicate; Effects of Temperature, Concentration, and Solvent on the Product Distribution of a Self-Assembly Process

William Cullen,[†] Christopher A. Hunter,[†,‡] and Michael D. Ward*[,†]

[†]Department of Chemistry, University of Sheffield, Sheffield S3 7HF, U.K.

[‡]Department of Chemistry, University of Cambridge, Lensfield Road, Cambridge CB2 1EW, U.K.

Supporting Information

ABSTRACT: The self-assembly between a water-soluble bis-bidentate ligand L^{18w} and Co(II) salts in water affords three high-spin Co(II) products: a dinuclear *meso*-helicate $[Co_2(L^{18w})_3]X_4$; a tetrahedral cage $[Co_4(L^{18w})_6]X_8$; and a dodecanuclear truncated-tetrahedral cage $[Co_{12}(L^{18w})_{18}]X_{24}$ (X = BF_4 or ClO_4). All three products were crystallized under different conditions and structurally characterized. In $[Co_2(L^{18w})_3]X_4$ all three bridging ligands span a pair of metal ions; in the two larger products, there is a metal ion at each vertex of the Co_4 or Co_{12} polyhedral cage array with a bridging ligand spanning a pair of metal ions along every edge. All three structural types are known: what is unusual here is the presence of all three from the same reaction. The assemblies **Co_2**, **Co_4**, and **Co_{12}** are in slow equilibrium (hours/days) in aqueous solution, and this can be conveniently monitored by ^{1}H NMR spectroscopy because (i) the paramagnetism of Co(II) disperses the signals over a range of ca. 200 ppm and (ii) the different symmetries of the three species give characteristically different numbers of independent ^{1}H NMR signals, which makes identification easy. From temperature- and concentration-dependent ^{1}H NMR studies it is clear that increasing temperature and increasing dilution favors fragmentation to give a larger proportion of the smaller assemblies for entropic reasons. High concentrations and low temperature favor the larger assembly despite the unfavorable entropic and electrostatic factors associated with its formation. We suggest that this arises from the hydrophobic effect: reorganization of several smaller complexes into one larger one results in a smaller proportion of the hydrophobic ligand surface being exposed to water, with a larger proportion of the ligand surface protected in the interior of the assembly. In agreement with this, ^{1}H NMR spectra in a nonaqueous solvent ($MeNO_2$) show formation of only $[Co_2(L^{18w})_3]X_4$ because the driving force for reorganization into larger assemblies is now absent. Thus, we can identify the contributions of temperature, concentration, and solvent on the result of the metal/ligand self-assembly process and have determined the speciation behavior of the **Co_2**/**Co_4**/**Co_{12}** system in aqueous solution.

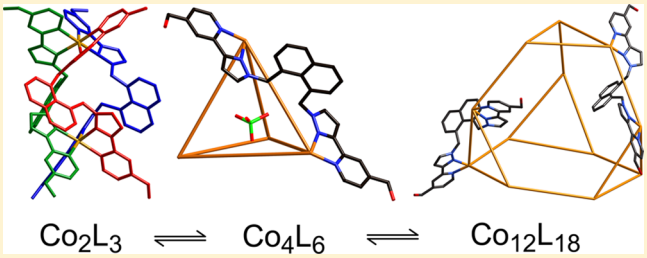

INTRODUCTION

The assembly of architecturally complex polyhedral coordination cages, from a combination of labile metal ions and relatively simple bridging ligands, has fascinated coordination chemists for more than 25 years.[1] From Saalfrank's early examples of M_4L_6 tetrahedral cages[2] to Fujita's recent $Pd_{24}L_{48}$ nanospheres,[3] the synthesis, structural characterization, and guest-binding properties of these hollow metal−organic capsules have provided deep insights into control of self-assembly as well as some useful examples of functional behavior arising from the host−guest chemistry.[1,4]

If a particular metal−ligand combination forms an assembly that is significantly more thermodynamically stable than the other possibilities, then a single product is formed and isolated, and will generally have the same structure in the solid state as it does in solution—behaving, in effect, like a conventional kinetically stable compound. This is very often the case, particularly when metal ions with strong stereoelectronic preferences (Pd^{2+}, Pt^{2+}) are combined with rigid bridging ligands that have a fixed, predictable arrangement of metal binding sites, as illustrated by work from the groups of Fujta,[1b,3] Stang,[5] and Shionoya.[6] In these cases, appropriate design of mutually complementary metal−ligand components can ensure that a single product is formed. In other cases, however, when flexible bridging ligands and/or metal ions with weaker stereochemical preference are used, numerous possible metal−ligand assemblies may be similar in energy with the result that different cages can form under different conditions, and two or more cages may exist in dynamic equilibrium in solution.[7]

This is the characteristic behavior of dynamic combinatorial libraries (DCLs).[8] In a DCL, there is generally a large number of possible products in equilibrium—the more the better. By a

Received: November 19, 2014
Published: February 20, 2015

DOI: 10.1021/ic502780b
Inorg. Chem. 2015, 54, 2626−2637

change in conditions, in particular addition of a template, it is possible to bias the equilibrium, amplifying one component of the library by binding to it and making it more stable. In the field of metallosupramolecular chemistry, prominent examples include mixtures of cyclic helicates of different sizes in which one component is amplified by a templating guest anion that binds strongly into the central cavity of whichever cyclic helicate in the mixture provides a cavity with the best size match.[9]

Dynamic mixtures of molecular polygons have come from the work of Fujita[7f] and Cotton.[7c] More elaborate examples of dynamic equilibria in metal complex assemblies include interconversion between a M_2L_3 dinuclear triple helicate and a M_4L_6 tetrahedron from Raymond's group[7j] and interconversion between large Ag(I)-based molecular grid and quadruple helicate structures from Lehn's group.[10] Recently Nitschke has developed large families of interconverting cages based on the same metal/ligand components whose equilibrium constitution can be controlled by changes in, for example, anion type and pH,[7i] and many other researchers have provided related examples of DCLs of metallosupramolecular assemblies.[7] Understanding and manipulating a complex equilibrium between many types of metal/ligand assemblies provides the next level of control in metallosupramolecular chemistry beyond the ligand design and choice of metal ion to give a specific assembly, which was the paradigm a few years ago.

Among our own family of coordination cages[1e,7a]—an extensive series based on combination of labile transition metal ions with bridging ligands containing pyrazolyl−pyridine chelating termini—we observed recently conversion between an $M_{16}L_{24}$ assembly, which formed in the solid state and was crystallographically characterized, and a smaller M_6L_9 assembly, which slowly formed in dilute solution when crystals of the $M_{16}L_{24}$ cage dissolved,[7a] with the interconversion triggered by the concentration change. In this contribution, we report a more elaborate equilibrium involving an interconversion between *three* different assemblies—an M_2L_3 cylindrical "mesocate" and M_4L_6 and $M_{12}L_{18}$ cages, all of which were structurally characterized. The position of the equilibrium is dependent on three variables (concentration, temperature, and solvent). We show how control of these parameters allows the equilibrium to be biased in favor of one component or another, using electrospray (ES) mass spectrometry (MS) and ^{1}H NMR spectroscopy to characterize the product distribution in solution.

RESULTS AND DISCUSSION

(i). Synthesis of Ligand and Complexes. We reported a while ago the assembly and structural characterization of the cage family $[M_{12}(L^{18naph})_{18}]X_{24}$ (M = Co, Cu, Cd, all in the 2+ state; $X^- = BF_4^-$ or ClO_4^-).[11] In these cages, as in all members of this family,[1e] a bridging ligand with two bidentate termini is combined with a six-coordinate metal ion, resulting in an assembly with a 2M/3L ratio that results in a polyhedral cage that has a 2:3 ratio of vertices to edges, with a metal ion occupying every vertex and a bridging ligand spanning a pair of metal ions along every edge. This has afforded (among others) M_4L_6 tetrahedra, M_6L_9 trigonal prisms, and M_8L_{12} cubes;[1e] the $[M_{12}(L^{18naph})_{18}]^{24+}$ cage cations have the form of truncated tetrahedra.[11] We have also found recently that making our cages water-soluble by addition of hydroxymethyl substituents to the external surface results in strong binding of hydrophobic guests in water, because the interior surface of the cage cavities is lined with CH groups from the ligand backbones and is therefore hydrophobic.[12] Seeking to extend this principle to the $[M_{12}(L^{18naph})_{18}]^{24+}$ cages, we prepared the hydroxymethyl-substituted ligand L^{18w} and prepared its Co(II) complex, expecting to obtain the water-soluble potential hosts $[Co_{12}(L^{18w})_{18}]X_{24}$ with a view to examining its host−guest properties.

The ligand synthesis is shown in Scheme 1 and follows a recently reported method.[12a] The key intermediate is

Scheme 1. Structural Formulae of the Ligands L^{18naph} and L^{18w} and the Synthetic Intermediates A and B

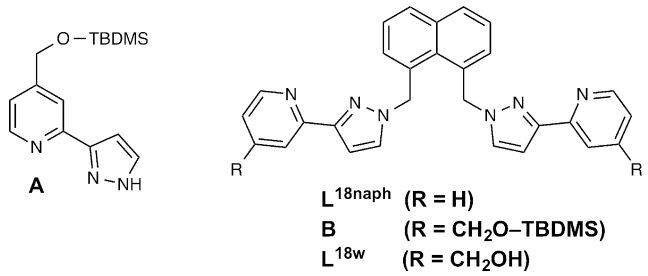

compound **A**, the chelating pyrazolyl−pyridine unit with a pendant *t*-butyl-dimethyl-silyl (TBDMS)-protected hydroxymethyl group at the pyridyl C^4 position. Reaction of this compound with 1,8-bis(bromomethyl)naphthalene, in the presence of NaH to remove the acidic pyrazole protons, afforded the TBDMS-protected ligand **B**; treatment with Bu_4NF liberated the hydroxy groups to afford L^{18w}. The crystal structure of $L^{18w}\cdot HBF_4$ is provided in Supporting Information.

We combined L^{18w} with $Co(BF_4)_2$ or $Co(ClO_4)_2$ in MeOH (3:2 molar ratio) and heated the mixture to 100 °C for 12 h in an autoclave, followed by slow cooling. This did not yield any crystals but gave an orange solution, which was evaporated to dryness. It was immediately obvious from ^{1}H NMR and ES MS measurements on the dried material that a complicated mixture of products had formed rather than a single species. The ^{1}H NMR spectrum showed a very large number of signals of varying intensity dispersed over the range from −120 to +100 ppm due to the paramagnetism of the high-spin Co(II) ions.[12,13] The mass spectrum was more informative and showed characteristic sequences of peaks corresponding to $\{Co_2(L^{18w})_3X_{4-n}\}^{n+}$, $\{Co_4(L^{18w})_6X_{8-n}\}^{n+}$, and $\{Co_{12}(L^{18w})_{18}X_{24-n}\}^{n+}$, plus other peaks that could not be assigned. Accordingly we looked at ways to isolate the individual components.

(ii). Structural Characterization of the Dinuclear Mesocate $[Co_2(L^{18w})_3](BF_4)_4$. Diffusion of diethyl ether vapor into a solution of the crude product (from the solvothermal synthesis) in $MeNO_2$ afforded crystals of what proved to be the dinuclear complex $[Co_2(L^{18w})_3](BF_4)_4$ (Figure 1; abbreviated hereafter as $\mathbf{Co_2}$) in which all three ligands span both metal centers. Superficially it looks like a triple helicate, but in fact the two metal centers within each molecule have opposed chirality so this is an example of a "meso-helicate" or *mesocate*, lacking helical chirality.[14] The conformation of the three ligands is clearly not the continuous spiral strand as seen in helicates; instead, there is a sharp bend in each ligand allowing one pyrazolyl−pyridine terminus to be angled in the opposite sense to the other. This allows the naphthyl group of each ligand to form a $\pi-\pi$ stacking interaction (separation 3.3−3.4 Å) with the coordinated

DOI: 10.1021/ic502780b
Inorg. Chem. 2015, 54, 2626−2637

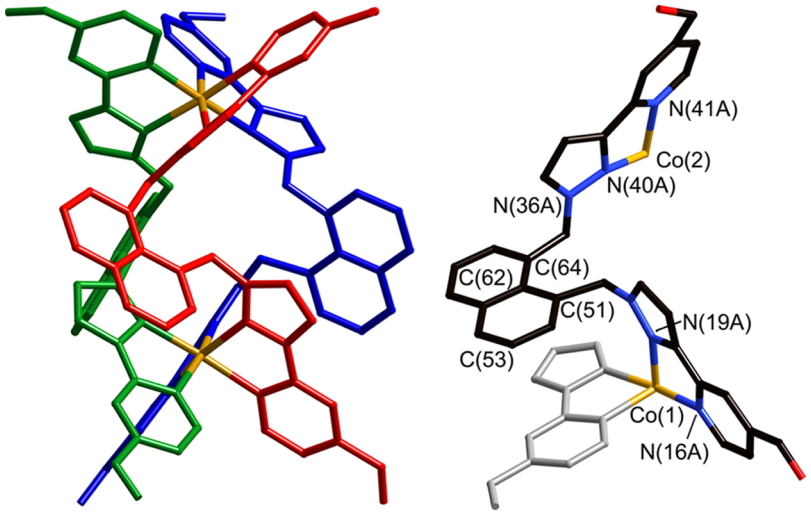

Figure 1. Two views of the complex cation of $[Co_2(L^{18w})_3](BF_4)_4$. (left) A view of the complete cation showing all three (equivalent) ligands colored separately. (right) A view showing the conformation of one ligand and the stacking at one end of the complex [around Co(1)] between the naphthyl groups of one ligands and the coordinated pyrazolyl−pyridine group of another.

Table 1. Crystal Parameters, Data Collection, and Refinement Details for the Structures in This Paper

complex	$[Co_2(L^{18w})_3](BF_4)_4$	$[Co_4(L^{18w})_6](ClO_4)_8{\cdot}18H_2O$	$[Co_{12}(L^{18w})_{18}](BF_4)_{24}{\cdot}1.5H_2O$	$L^{18w}{\cdot}HBF_4{\cdot}2CHCl_3$
formula[a]	$C_{90}H_{78}N_{18}B_4Co_2F_{16}O_6$	$C_{180}H_{192}N_{36}Cl_8Co_4O_{62}$	$C_{540}H_{471}N_{108}B_{24}Co_{12}\ F_{96}O_{37.5}$	$C_{32}H_{29}BCl_6F_4N_6O_2$
molecular weight	1972.8	4371.0	11 863.8	829.12
T, K	100(2)	100(2)	100(2)	100(2)
crystal system	trigonal	triclinic	trigonal	triclinic
space group	$R\bar{3}c$	$P\bar{1}$	$R\bar{3}$	$P\bar{1}$
a, Å	18.885(3)	19.2188(13)	44.705(9)	9.5725(3)
b, Å	18.885(3)	29.070(2)	44.705(9)	11.1173(3)
c, Å	101.44(2)	35.460(3)	68.621(14)	17.7204(5)
α, deg	90	90.322(3)	90	83.021(2)
β, deg	90	98.971(3)	90	77.285(2)
γ, deg	120	98.598(3)	120	84.835(2)
V, Å^3	31 333(11)	19 340(2)	118 768(54)	1813.47(9)
Z	12	4	6	2
ρ, g cm^{-3}	1.255	1.501	0.995	1.518
crystal size, mm^3	0.22 × 0.08 × 0.03	0.18 × 0.11 × 0.05	0.1 × 0.1 × 0.1	0.35 × 0.33 × 0.08
data, restraints, parameters	4534, 463, 335	88 225, 5308, 4968	23 528, 2282, 1767	6141, 0, 462
final $R1$, $wR2$[b]	0.188, 0.519	0.128, 0.406	0.199, 0.522	0.044, 0.112

[a]These formulas (and consequently the crystal densities) are necessarily approximate given that large amounts of diffuse electron density in solvent-accessible voids was removed from the refinements using either the "SQUEEZE" function in PLATON or the OLEX "Solvent Mask" function. See CIFs, and comments in Experimental Section, for details. [b]The value of $R1$ is based on "observed" data with $I > 2\sigma(I)$; the value of $wR2$ is based on all data.

pyrazolyl−pyridine group from another ligand—a typical interaction between parallel and overlapping electron rich and electron deficient aromatic fragments, of the sort that is commonplace in this family of complexes.[1e,11,12] All three such interactions are at the same end of the complex, with the three pyrazolyl−pyridine units around Co(1) all forming stacking interactions with adjacent naphthyl groups; this cannot happen around the other terminus [Co(2)] without a substantial change in the ligand conformations. Thus, the stacking interactions appear to "lock" the ligands in an asymmetric conformation with two inequivalent termini. Bond distances around the Co(II) ions are unremarkable and characteristic of high-spin Co(II), lying in the range of 2.12−2.17 Å. The Co(1)···Co(2) separation is 7.85 Å. A space-filling view is shown in Supporting Information. Crystallographic data are summarized in Table 1.

The result is that the complex cation has 3-fold rotational symmetry with the axis passing through both *fac* tris-chelate metal centers. However, the absence of 2-fold symmetry within each ligand means that the molecular symmetry is just C_3, rather than D_3 as is normally seen in triple helicates when the ligands each have 2-fold symmetry with equivalent termini. This is comparable to the situation that occurs in triple helicates of nonsymmetrical ditopic ligands that have different "head" and "tail" ends, with the three ligands aligned in a "head-to-head-to-head" manner.[15]

The 3-fold molecular symmetry means that, if this structure is preserved in solution, we expect to see one ligand environment but with no internal symmetry, that is, 24 independent signals in the ^{1}H NMR spectrum (not including the exchangeable OH protons). This assumes that the protons of the two methylene groups are diastereotopic in the local chiral environment around each tris-chelate metal center and

DOI: 10.1021/ic502780b
Inorg. Chem. 2015, 54, 2626−2637

will therefore give separate signals. The ^{1}H NMR spectrum of a solution prepared from freshly dissolved crystals of **Co$_2$** in D_2O was consistent with this (Figure 2), with 24 signals apparent in

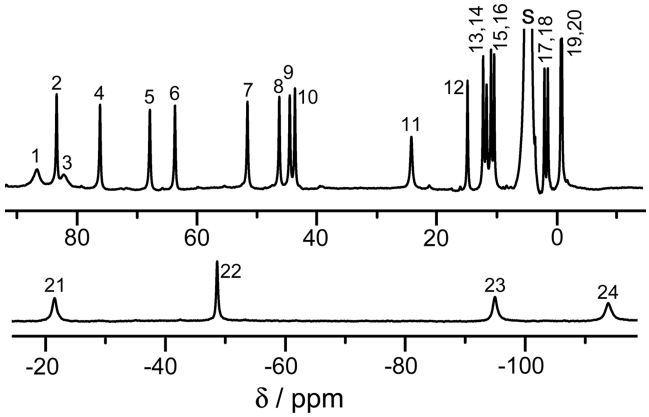

Figure 2. 400 MHz ^{1}H NMR spectrum (D_2O, 298 K) of redissolved crystals of $[Co_2(L^{18w})_3](BF_4)_4$. All 24 expected signals are resolved and numbered; "S" denotes the signal from residual protonated solvent.

the range from −120 to +90 ppm. The signals have not been individually assigned but—as we have seen in other ^{1}H NMR spectra of high-spin Co(II) cages[13b,c]—the broad, less intense peaks are from the protons with a short t_1 value due to their proximity to the paramagnetic centers, and the sharper, more intense signals arise from the protons further from the metal centers. As usual, individual ^{1}H−^{1}H couplings are not resolved. The key point is that the number of signals in this spectrum is exactly what we would expect from the C_3-symmetric solution structure. By analogy with previously reported spectra, for example, we can say that the two weak, broad signals between 80 and 90 ppm (signals 1 and 3) are from the pyridyl H^6 protons of the two similar but inequivalent termini of L^{18w},[13b,c] and the four signals at negative chemical shift (pairs of signals 21/22 and 23/24) are from the two inequivalent methylene groups, each of which is diastereotopic. The presence of signals in pairs—corresponding to the two halves of the ligand being in two slightly different chemical environments—is particularly clear for the four pairs of signals numbered 13−20 in Figure 2.

The ES mass spectrum of freshly dissolved crystals shows the sequence of peaks corresponding to the species $\{Co_2(L^{18w})_3(X)_{4-n}\}^{n+}$ (n = 1, 2, 3, 4) with correct isotopic spacings in each case and correct accurate mass measurements on selected signals (see Supporting Information).

(iii). Structural Characterization of the Tetrahedral Cage $[Co_4(L^{18w})_6](ClO_4)_8$. Slow cooling of a solution of the crude reaction mixture in D_2O afforded crystals of what proved to be the tetrahedral cage $[Co_4(L^{18w})_6](ClO_4)_8$ (Figure 3, hereafter abbreviated **Co$_4$**). This has a *fac* tris-chelate metal ion at each vertex of the tetrahedron, and a bridging ligand spanning a pair of metal ions along each of the six edges.[11a,13b,16] The naphthyl group of each bridging ligand forms π-stacking interactions with the coordinated pyrazolyl−pyridine termini of two other ligands, forming a three-component A/D/A sandwich (A = electron-deficient pyrazolyl−pyridine acceptor unit, D = electron-rich naphthyl donor unit) along every edge of the tetrahedron. As is usually the case in these tetrahedral cages, an anion occupies the central cavity.[11a,13b,16] This guest anion is inverted with respect

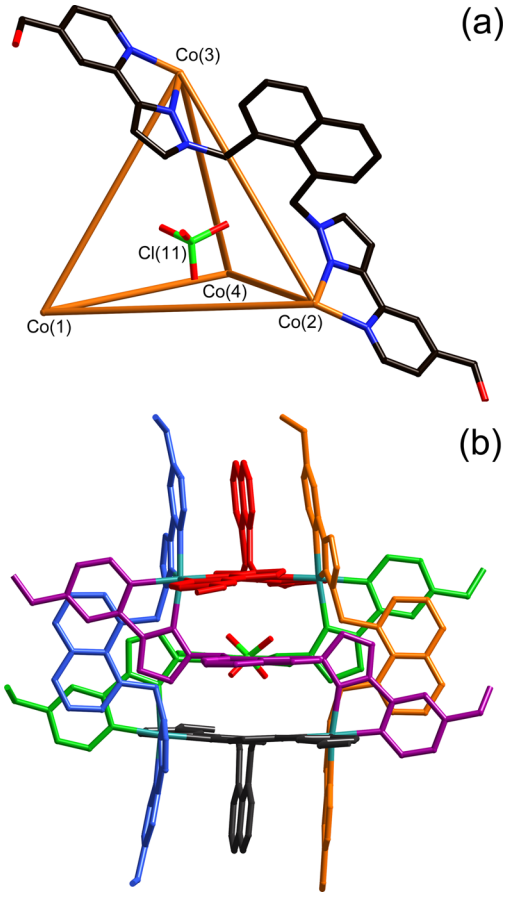

Figure 3. Two views of the complex cation of $[Co_4(L^{18w})_6](ClO_4)_8$. (a) A view emphasizing the tetrahedral topology, with a metal ion at each vertex, a bridging ligand spanning each edge, and the presence of an encapsulated perchlorate ion guest, which is inverted with respect to the Co_4 tetrahedron. (b) A view of the complete complex cation with each of the six ligands colored separately, emphasizing the π-stacking in which every electron-rich naphthyl group is sandwiched between two electron-deficient coordinated pyrazolyl−pyridine units.

to the cage tetrahedron such that each O atom of the perchlorate guest is oriented toward the space in the center of one of the triangular faces of the Co_4 tetrahedral array. The anion is involved in CH···O hydrogen-bonding interactions with the interior surface of the cage, with numerous nonbonded H···O separations in the range of 2.6−2.7 Å, and the associated C···O separations being ca. 3.2−3.3 Å. The Co···Co separations along the edges of the cage cations are in the range of 9.34−9.60 Å (average 9.53 Å), and the Co−N separations are again in the range of 2.11−2.19 Å. A space-filling view is in Supporting Information.

Although there are two crystallographically independent complex molecules, each with no internal symmetry, in the asymmetric unit, in solution the loss of symmetry from crystal packing is relaxed, and the ^{1}H NMR spectrum in D_2O is consistent with the complex having T symmetry (Figure 4). This arises from the presence of four C_3 axes (one through each metal center) and three C_2 axes (bisecting each opposed pair of ligands). This means that the two halves of each ligand are magnetically equivalent, and the ^{1}H NMR spectrum accordingly contains only 12 signals (excluding exchangeable OH protons) between −80 and +90 ppm. By inspection the spectrum is clearly only half as complex as that of **Co$_2$** in Figure

DOI: 10.1021/ic502780b
Inorg. Chem. 2015, 54, 2626−2637

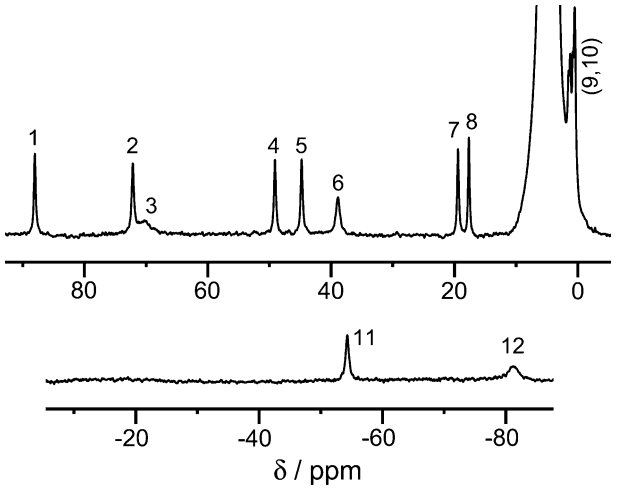

Figure 4. 400 MHz ^{1}H NMR spectrum (D_2O, 298 K) of redissolved crystals of $[Co_4(L^{18w})_6](ClO_4)_8$. Of the 12 expected signals, 10 are clear (1–8, 11, and 12) and the other two (9, 10) are overlapping close to the residual broad protonated solvent peak centered at ~5 ppm.

2, with—for example—only a single pyridyl H^6 signal (No. 3) and a single signal for each of the diastereotopic methylene protons (signals 11 and 12). The integrity of the complex in solution was also confirmed by the ES mass spectrum, which showed a series of peaks corresponding to the species $\{Co_4(L^{18w})_6(ClO_4)_{8-n}\}^{n+}$ (n = 2, 3, 4); see Supporting Information. The signal at m/z 913 for $\{Co_4(L^{18w})_6(ClO_4)_4\}^{4+}$ could be distinguished from the signal for $\{Co_2(L^{18w})_3(ClO_4)_2\}^{2+}$ at the same m/z value (from **Co_2**) by its isotopic pattern and the spacing of 0.25 units, instead of 0.5 units, between adjacent components of the isotope sequence. The same applies to all other signals, making assignments unambiguous.

(iv). Structural Characterization of the Truncated Tetrahedral Cage $[Co_{12}(L^{18w})_{18}](BF_4)_{24}$. We were unable to isolate the larger component—tentatively identified as dodecanuclear $[Co_{12}(L^{18w})_{18}](BF_4)_{24}$ from the mass spectrum of the crude material—from the initially obtained mixture by fractional crystallization, so we sought to effect chromatographic purification. On the basis that any dodecanuclear complex would be much larger than the dinuclear and tetranuclear species identified so far, we used size-exclusion chromatography with Sephadex G-50, eluting with water. The column developed as a well-defined orange band that eluted first and was shown to be pure $[Co_{12}(L^{18w})_{18}]X_{24}$ by mass spectrometry; this band was followed by a more diffuse orange band containing the smaller complexes, which did not separate under these conditions.

Concentrating and cooling the aqueous solution of the initial fraction afforded crystals of what proved to be the initially expected truncated-tetrahedral complex $[Co_{12}(L^{18w})_{18}](BF_4)_{24}$ (Figure 5). This has the general structure that we have seen before in complexes of the parent ligand L^{18naph}.[11] The truncated tetrahedron is an Archimedean solid with all vertices equivalent, but two types of faces—triangular and hexagonal—and two types of edge. The two types of edge may be described as type ***a***, which are the 12 edges associated with the four triangular faces, and type ***b***, which are the six edges connecting these triangles—these are the edges of the parent tetrahedron before it was truncated. The ligands spanning these edges may

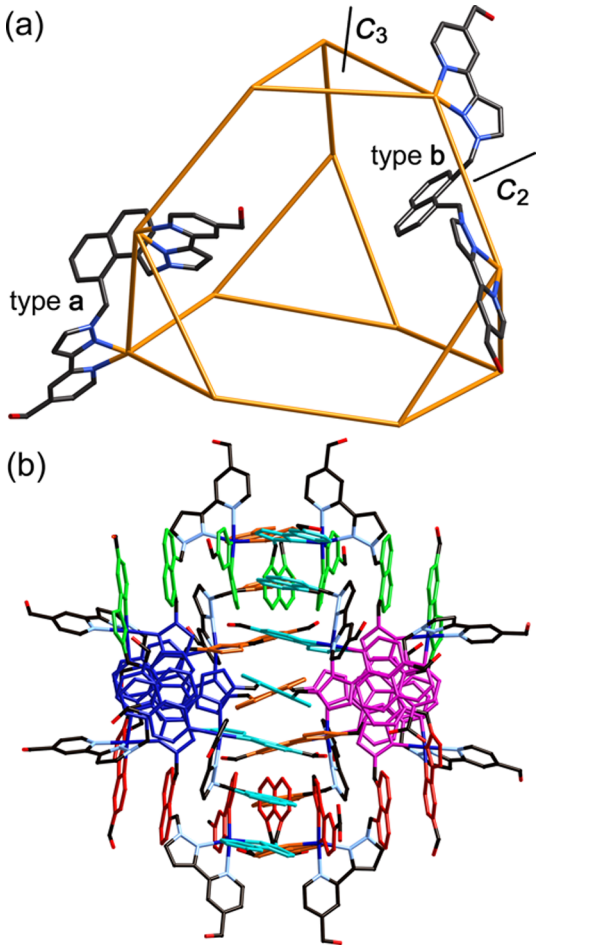

Figure 5. Two views of the complex cation of $[Co_{12}(L^{18w})_{18}](BF_4)_{24}$. (a) A view emphasizing the truncated tetrahedral topology, with a metal ion at each vertex and a bridging ligand spanning each edge, and the presence of two different ligand environments according to whether the ligand spans an edge of a triangular (type ***a***) or one of the edges linking two triangular faces (type ***b***). 3-Fold and 2-fold rotation axes are also illustrated. (b) A view of the complete complex cation with the six π-stacked arrays—each of which contains a seven-component alternating array of pyrazolyl–pyridine and naphthyl components—colored separately.

therefore be abbreviated as L^a, of which there are 12 (with no internal symmetry), and L^b, of which there are six (lying on a 2-fold axis). Each $M_3(L^a)_3$ triangular face is a cyclic helicate, with four of these linked in a tetrahedral array by additional bridging ligands. All metal centers in this structure are meridional tris-chelates—in contrast to the first two structures—and all metal centers are homochiral. The arrangement of ligands, and in particular the flexibility associated with the methylene groups that link the pyrazolyl-pyridine termini to the central aromatic core, permits extensive aromatic stacking (Figure 5b) with six seven-membered A-D-A-D-A-D-A stacks around the periphery of the complex, where (as before) A denotes an electron-deficient pyrazolyl–pyridine acceptor, and D denotes an electron-rich naphthyl donor. Co–N distances are in the range of 2.09–2.23 Å, and Co···Co separations are in the range of 9.35–9.53 Å (average 9.45 Å).

The spaces in the center of each triangular and hexagonal face provide a pocket that accommodates a tetrafluoroborate anion that forms CH···F interactions with the surrounding ligand; thus, eight anions are associated with the surface of the

DOI: 10.1021/ic502780b
Inorg. Chem. 2015, 54, 2626–2637

cage. The central cavity probably also contains a combination of anions and/or solvent molecules, but these were severely disordered and could not be modeled successfully in the crystallographic refinement. Additional views of the structure are in Supporting Information.

In the absence of crystal packing effects, we expect again that in solution this complex cation will have *T* symmetry, which is a common consequence of removing symmetry planes from point groups of higher-symmetry polyhedra.[17] There is a C_3 axis through the center of each $M_3(L^a)_3$ triangular face (and also through the opposite hexagonal face), as well as three C_2 axes, each of which bisects an opposite pair of L^b ligands along the type ***b*** edges. The result of this is that there must be 1.5 magnetically independent ligand environments. In the 12 L^a ligands, all protons are inequivalent due to the helical chirality of the $M_3(L^a)_3$ triangular array, which means that the ligands have distinct "head" and "tail" ends. The six L^b ligands are all bisected by C_2 axes, generating 12 equivalent halves of the L^b-type ligands. The result is 36 magnetically inequivalent protons with the same abundance (excluding exchangeable OH protons), and the ^{1}H NMR spectrum is consistent with this (Figure 6). The spectrum at 298 K was noticeably broader and

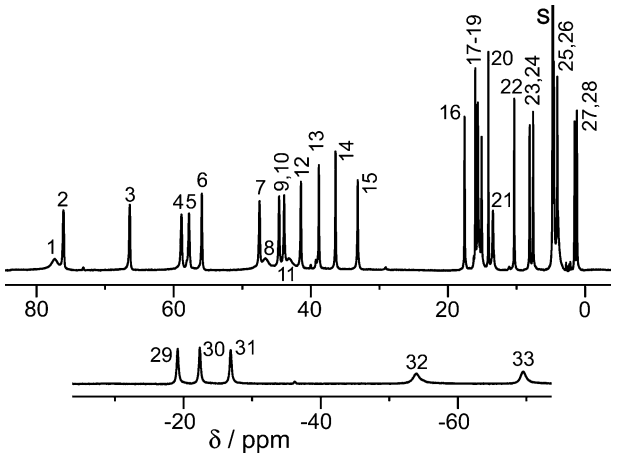

Figure 6. 400 MHz ^{1}H NMR spectrum (D_2O, 90 °C) of redissolved crystals of $[Co_{12}(L^{18w})_{18}](BF_4)_{24}$. Of the 36 expected signals, 33 are clear. The others are assumed to be either obscured by the residual protonated solvent peak (**S**) or too broad to detect (see main text).

less well-resolved than those of $\mathbf{Co_2}$ and $\mathbf{Co_4}$ at the same temperature, presumably due to the slow tumbling of the large molecule in solution, which broadens the spectrum above and beyond the effects of paramagnetism. Warming the solution sharpened the signals, and Figure 6 shows the ^{1}H NMR spectrum at 90 °C. We can now easily identify 33 of the expected 36 signals; the missing ones may be obscured under the HOD peak (there are many closely spaced signals in this region) or may still be too broad to detect. However, this spectrum is clearly in agreement with the symmetry of the solid-state structure, and in particular we can see how some signals occur in sets of three corresponding to the three independent ligand halves [e.g., broad signals 1, 8, and 11 in Figure 6 are the three pyridyl H^6 environments, and signals 29–31 arise from one of the protons on each of the three independent methylene groups]. The ES mass spectrum (see Supporting Information) confirms the integrity of the cage in aqueous solution, showing a sequence of seven peaks from the species $\{Co_{12}(L^{18w})_{18}(BF_4)_{24-n}\}^{n+}$ (n = 6–12 inclusive) formed by successive loss of tetrafluoroborate anions.

(v). Interconversion between the Structures in Aqueous Solution: Effects of Temperature. Since multiple attempts at changing the experimental conditions for the synthesis results in a similar mixture of components in every case, the possibility suggests itself that the different species isolated as crystals could be in slow equilibrium—as we have seen in one other case.[7a] The fact that we could obtain clean ^{1}H NMR spectra of each species independently from redissolved crystals means that any equilibrium must be on a time scale of hours or longer at room temperature, which made separation and individual identification of the components possible (e.g., we could isolate pure $\mathbf{Co_{12}}$ by size-exclusion column chromatography). ^{1}H NMR spectroscopy provides a convenient tool to study any equilibration between components, in particular because (i) the paramagnetism disperses the signals over such a wide chemical shift range, such that most individual signals are clearly resolved;[13] and (ii) the different symmetries result in different numbers of independent signals for each complex (12, 24, or 36), which allows each set of signals to be identified easily. The NMR studies were performed using the $[BF_4]^-$ salts (except where we needed pure crystalline $\mathbf{Co_4}$, for which we used redissolved crystals of the $[ClO_4]^-$ salt). In aqueous solution the nature of the anion makes no difference to the complex structure as it is solvated; the perchlorate and tetrafluoroborate salts of a given complex cation gave the same ^{1}H NMR spectra in water.

Initially we examined the effect of temperature. A solution of some of the initially isolated crude mixture of complex products (6 mg in 0.6 mL of D_2O) was prepared, and the ^{1}H NMR spectrum was recorded at 25 °C; the mixture at this point contained mainly the $\mathbf{Co_{12}}$ and $\mathbf{Co_4}$ species (Figure 7).

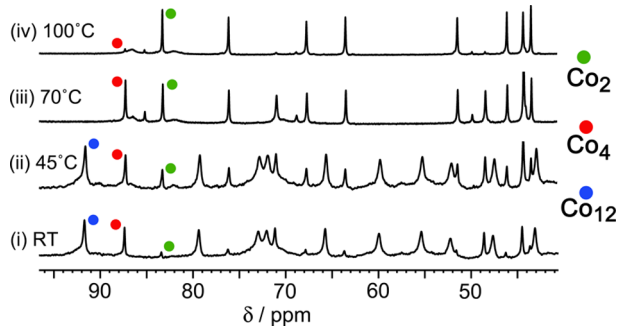

Figure 7. Partial ^{1}H NMR spectra of the as-isolated mixture of complexes ($[BF_4]^-$ salts) after equilibration of the sample (6 mg in 0.6 cm^3 of D_2O, corresponding to total Co concentration of 10^{-2} M) at (i) RT, (ii) 45, (iii) 70, and (iv) 100 °C.

Warming the solution to 45 °C resulted in some changes in relative intensity of different components, so the solution was held at this temperature until no further changes occurred (4 d). At this temperature, we saw that weak signals due to the M_2 complex had appeared. At 70 °C, the solution needed only 1 d before equilibrium was reached. This spectrum showed a large change in the composition of the mixture: the major species were now $\mathbf{Co_4}$ and $\mathbf{Co_2}$, with none of the $\mathbf{Co_{12}}$ complex present. Finally the temperature was raised to 100 °C, and the sample was monitored by ^{1}H NMR spectroscopy until a new equilibrium had been reached (12 h). At this temperature, not only had the $\mathbf{Co_{12}}$ species disappeared, but there was very little

DOI: 10.1021/ic502780b
Inorg. Chem. 2015, 54, 2626–2637

of the Co_4 complex, with the Co_2 complex being the dominant species. Allowing the mixture to cool to 25 °C re-established the initial equilibrium composition after 3 d. These spectroscopic changes are summarized in Figure 7.

We prepared a solution that was *not* at equilibrium by dissolving crystals of Co_2 in D_2O to give the same total concentration of Co(II) ions as before. The initial ^1H NMR spectrum at 25 °C was that of pure Co_2 (cf. Figure 2). However, the spectrum slowly changed, with the signals characteristic of Co_4 and Co_{12} growing in intensity until equilibrium was established after ~36 h (Figure 8). At this

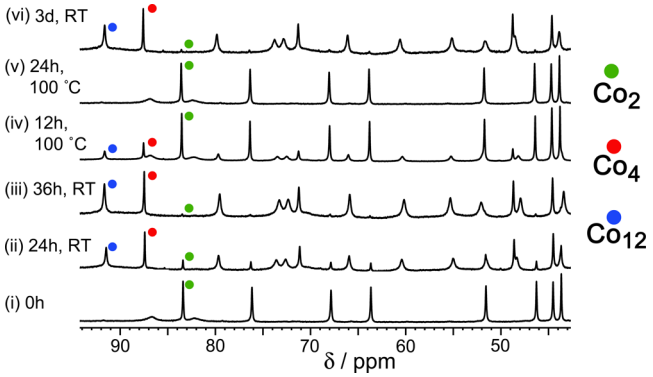

Figure 8. Partial ^1H NMR spectra showing the evolution of the mixture of complexes under different conditions, starting with redissolved crystals of Co_2 [6 mg in 0.6 cm^3 of D_2O; spectrum (i)]. Spectra (ii) and (iii) show the equilibrium slowly being established at RT, with spectrum (iii) being similar to the first spectrum of Figure 7 (the as-isolated mixture of complexes at RT). Spectra (iv) and (v) show the change in composition toward almost completely pure Co_2 over 24 h as the temperature is increased to 100 °C; spectrum (vi) shows that cooling the sample to RT results in the previous equilibrium of spectrum (iii) being re-established.

point the composition of the mixture was identical to that obtained above from the crude reaction mixture at 25 °C. Increasing the temperature to 100 °C and then recooling, allowing appropriate equilibration time at each stage, resulted in the same evolution of spectra as seen before (Figure 7). Similar experiments using redissolved crystals of pure Co_4 or Co_{12} [again, with the same total concentration of Co(II) ions] gave the same results: the initially obtained spectrum of pure complex in each case evolved slowly to show the same equilibrium mixture of Co_2, Co_4, and Co_{12} appropriate to the temperature. Thus, we see identical behavior in solution whether we start from the as-isolated mixture of complex components or from redissolved crystals of *any one component*, proving that the $Co_2/Co_4/Co_{12}$ system exists in aqueous solution as a fully reversible equilibrium.

Fragmentation of Co_{12} into a larger number of smaller complexes is entropically favorable, so as the temperature increases the value of $T\Delta S°$ increases, and the equilibrium shifts toward Co_4 and Co_2. In addition, this fragmentation disperses the positive charges over more particles, which is electrostatically favorable.

This raises the question of why the larger assemblies form at all: there must be an additional factor specifically favoring formation of Co_{12} in preference to six molecules of Co_2 or three molecules of Co_4. Many of the specific interactions that contribute to $\Delta H°$ for formation of an individual complex scale linearly with complex size so do not provide a driving force for formation of larger assemblies. For example, the total number of metal–ligand bonds is independent of the size of the assembly: one Co_{12} complex contains the same number of Co–N bonds (of similar length, according to the crystal structures, and therefore similar strength) as three Co_4 complexes or six Co_2 complexes. Similarly, there are more pairwise $\pi-\pi$ stacking interactions in larger assemblies, but the crystal structures show 12 such interactions in Co_4 and 36 in Co_{12}, so the number of $\pi-\pi$ stacking interactions is two per ligand in each case.

The main systematic structural change that would favor formation of larger assemblies is a decrease in the surface area to volume ratio: the larger the assembly, the smaller is the proportion of hydrophobic ligand backbone that is exposed to water at the surface, and the greater is the proportion that is buried in the interior and protected from solvent. Thus, the hydrophobic effect systematically favors larger assemblies.[18] We can estimate the surface areas of the complexes by using the X-ray crystal structures. Using a water molecule as the probe, the solvent-accessible surface areas of the complex cations of Co_4 and Co_{12} are 2076 and 4885 $Å^2$, respectively. Thus, three complex cations of Co_4 have an external surface area of ca. 6200 $Å^3$ in contact with the aqueous solvent, and reorganizing them into a single Co_{12} complex cation reduces the hydrophobic surface area by ca. 1300 $Å^3$, providing a strong driving force for formation of the larger assembly in water.[19] This competition between an increased hydrophobic effect, which promotes larger assemblies, with other entropic/electrostatic factors promoting fragmentation into smaller assemblies, qualitatively explains the concentration and temperature dependence of the equilibrium composition of the $Co_2/Co_4/Co_{12}$ mixture in aqueous solution.

(vi). Effect of Changing Solvent. Our hypothesis that the hydrophobic effect drives formation of the larger assemblies by minimizing the solvent-accessible surface area is easily tested by measuring ^1H NMR spectra in nonaqueous solvents. The complexes are poorly soluble in anything except water. However, a saturated solution of the as-isolated reaction mixture in CD_3NO_2 at 25 °C (ca. 1 mg in 0.6 cm^3 of solvent), allowed to equilibrate for several days, showed the presence of only Co_2 (Figure 9a). The spectrum was weak and noisy, but in

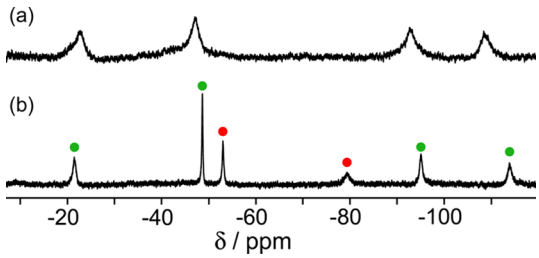

Figure 9. Partial ^1H NMR spectra at 25 °C of the crude reaction product [$(BF_4)^-$ salt; 1 mg in 0.6 cm^3 of solvent]: (a) in CD_3NO_2, showing the presence of only Co_2 (compare with Figure 2), and (b) in D_2O, showing the presence of a mixture of Co_2 (green ●) and Co_4 (red ●) (compare with Figures 2 and 4).

the negative chemical shift region we can clearly see that there are four signals consisting of two protons in two different environments, exactly similar to what we see for Co_2 in aqueous solution (Figure 2) and inconsistent with formation of either of the larger complexes. ES mass spectra of the saturated solution of Co_2 in CD_3NO_2 agreed with this, with signals for Co_2—but none for Co_4 or Co_{12}—being apparent. This solution was then

DOI: 10.1021/ic502780b
Inorg. Chem. 2015, 54, 2626–2637

evaporated to dryness and redissolved in 0.6 cm^3 of D_2O, to allow comparison of the ^1H NMR spectra between the two solvents at the same concentration. After a few days to allow the solution to equilibrate at room temperature (RT), the ^1H NMR spectrum in D_2O (Figure, 9b) showed that *both* $\mathbf{Co_2}$ and $\mathbf{Co_4}$ were present, as illustrated by the appearance of six signals in the negative chemical shift region, four from $\mathbf{Co_2}$ and two from $\mathbf{Co_4}$, exactly matching the corresponding signals in Figures 2 and 4. This solution was too dilute to allow formation of any $\mathbf{Co_{12}}$ (see next section), but the general behavior is clear: in a nonaqueous solvent, only $\mathbf{Co_2}$ can be detected because the hydrophobic effect, which is the driving force for assembly of $\mathbf{Co_4}$ and $\mathbf{Co_{12}}$ in water, disappears. Indeed we could only obtain crystals of $\mathbf{Co_2}$ from $MeNO_2$ solution—all crystallizations from aqueous solution afforded either $\mathbf{Co_4}$ or $\mathbf{Co_{12}}$.

(vii). Interconversion between the Structures in Aqueous Solution: Effects of Concentration. We also examined the effect of concentration on the equilibrium between the three species in water. We repeated the series of experiments described above at different temperatures (25, 45, 70, and 100 °C) but using a solution that was 10 times more concentrated (60 mg of material in 0.6 cm^3 of D_2O). The difference was striking (Figure 10). At 25 °C, the higher

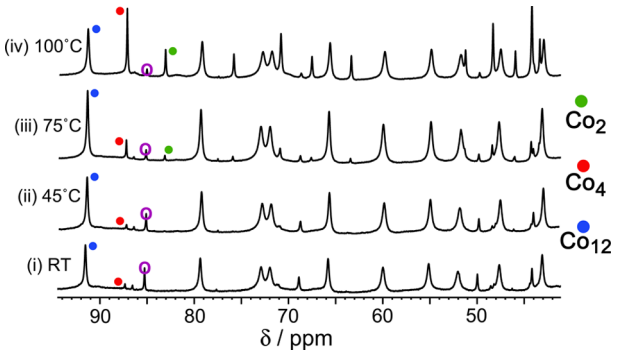

Figure 10. A repeat of the experiment in Figure 7, but using a concentration 10 times higher (60 mg of as-isolated complex mixture in 0.6 cm^3 of D_2O, corresponding to total Co concentration of 0.1 M). The shift in the equilibrium composition (compared to the more dilute solution) at each temperature toward the larger complexes is clear. The purple circle denotes an unidentified complex that is not detectable at lower concentrations, which we believe to be a complex with nuclearity > $\mathbf{Co_{12}}$ on the basis of its concentration and temperature dependence (see main text).

concentration resulted in the solution at equilibrium containing almost entirely $\mathbf{Co_{12}}$, with $\mathbf{Co_4}$ and $\mathbf{Co_2}$ being barely detectable. As before, as the temperature increased, the amount of $\mathbf{Co_{12}}$ diminished, and the amounts of $\mathbf{Co_4}$ and $\mathbf{Co_2}$ increased; at 100 °C all three components were present in significant amounts (Figure 8). This result contrasts with the dilute solution in which $\mathbf{Co_2}$ dominated at 100 °C (Figure 7).

This is a manifestation of basic principles of equilibria when there are different numbers of species on either side of the process. Consider the equilibrium between three molecules of $\mathbf{Co_4}$ and one of $\mathbf{Co_{12}}$ (eq 1).

$$3Co_4 \rightleftharpoons Co_{12} \quad (1)$$

$$[Co_{12}] = K[Co_4]^3 \quad (2)$$

The associated equilibrium constant (eq 2) shows that, as the total concentration increases, the balance will quickly shift toward the larger complex. A factor of 10 increase in the equilibrium concentration of $\mathbf{Co_4}$ requires a factor of 1000 increase in the concentration of $\mathbf{Co_{12}}$ to maintain the equilibrium constant, that is, the $[\mathbf{Co_{12}}]/[\mathbf{Co_4}]$ ratio will increase by a factor of 100. Similarly, in the $2\mathbf{Co_2} \rightleftharpoons \mathbf{Co_4}$ equilibrium, increasing the concentration of $\mathbf{Co_2}$ by a factor of 10 requires $[\mathbf{Co_4}]$ to increase by a factor of 100, that is, a factor of 10 increase in the $[\mathbf{Co_4}]/[\mathbf{Co_2}]$ ratio. A shift in concentration domain by a factor of 10—as per the difference between spectra in Figures 7 and 8—therefore strongly increases the proportions of the larger complexes present in the equilibrium mixture.

Apart from the signals in the ^1H NMR spectrum assignable to $\mathbf{Co_2}$, $\mathbf{Co_4}$, and $\mathbf{Co_{12}}$, at the high concentration/low temperature limit, we can see evidence of additional weak signals (shown in purple in Figure 10), which do not correspond to any of the three known species. These signals decrease in intensity at higher temperature. The appearance of signals that are only present at high concentrations and low temperatures is consistent with a small amount of an as-yet unidentified species that is even larger than $\mathbf{Co_{12}}$. We could not identify this complex by mass spectrometry of the high concentration/low temperature mixture. We note, however, that we have identified (with different bridging ligands) examples of $M_{16}L_{24}$ assemblies in this cage family, so this additional species might be an assembly of that nature.[7a,20]

(viii). Calculation of Speciation Behavior for the Co_2/Co_4/Co_{12} System in Aqueous Solution. From integration of signals associated with different species in the equilibrium we can determine their relative concentrations. This requires careful consideration of the symmetry of the complexes, as a single signal corresponds to a different number of protons in each case. In $\mathbf{Co_2}$ one signal corresponds to 3H as there are three equivalent ligands with no internal symmetry; in $\mathbf{Co_4}$, with six equivalent ligands all having 2-fold symmetry, each signal corresponds to 12H; and in $\mathbf{Co_{12}}$, with 18 ligands split into 12 equivalent sets (each of 1.5 magnetically equivalent ligands), each signal again corresponds to 12H. Taking this into account, and knowing the total amount of complex used, we can calculate the concentration of each species. From the set of spectra at 25 °C we obtain, for the $2\mathbf{Co_2} \rightleftharpoons \mathbf{Co_4}$ equilibrium, an equilibrium constant of 8.4×10^3 M^{-1} ($\Delta G° = -22$ kJ mol^{-1}); and for the $3\mathbf{Co_4} \rightleftharpoons \mathbf{Co_{12}}$ equilibrium, we obtain an equilibrium constant of 1.5×10^7 M^{-2} ($\Delta G° = -41$ kJ mol^{-1}). These values are averaged from several NMR measurements at different concentrations. From these equilibrium constants, we see that for the $6\mathbf{Co_2} \rightleftharpoons \mathbf{Co_{12}}$ equilibrium, the equilibrium constant is 9.1×10^{18} M^{-5} [$\Delta G = 108$ kJ mol^{-1}, i.e., $3(-22) + (-41)$ kJ mol^{-1} within rounding errors]. Table 2 lists the equilibrium

Table 2. Equilibrium Constants for Interconversions between Co_2, Co_4, and Co_{12} at Different Temperatures Based on Integration of Signals in ^1H NMR Spectra[a]

temperature, °C	K_{2-4}, M^{-1}	K_{4-12}, M^{-2}	K_{2-12}, M^{-5}
25	8.4×10^3	1.5×10^7	9.1×10^{18}
45	2.8×10^3	4.8×10^7	1.1×10^{18}
70	7.4×10^2	2.1×10^7	8.7×10^{15}
100	3.6×10^2	1.0×10^7	4.6×10^{14}

[a]Equilibrium constant K_{2-4} is for the $2\mathbf{Co_2} \rightleftharpoons \mathbf{Co_4}$ equilibrium; K_{4-12} is for the $3\mathbf{Co_4} \rightleftharpoons \mathbf{Co_{12}}$ equilibrium; and K_{2-12} is for the $6\mathbf{Co_2} \rightleftharpoons \mathbf{Co_{12}}$ equilibrium. Hence $K_{2-12} = [K_{2-4}]^3[K_{4-12}]$.

DOI: 10.1021/ic502780b
Inorg. Chem. 2015, 54, 2626−2637

constants at four different temperatures (25, 45, 70, and 100 °C). From these equilibrium constants, we can determine the speciation behavior for the whole three-component system at a range of temperatures, as shown in Figure 11. The accuracy of

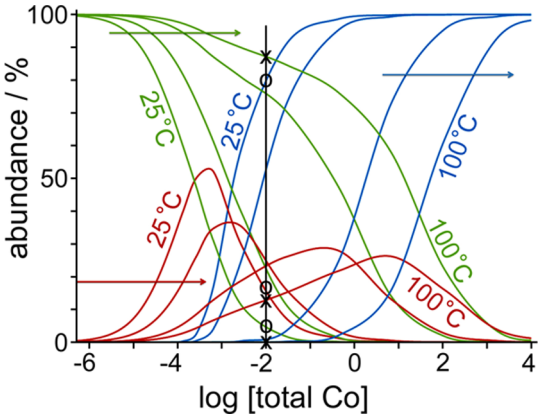

Figure 11. Speciation behavior of the $\mathbf{Co_2}$ (green)/$\mathbf{Co_4}$ (red)/$\mathbf{Co_{12}}$ (blue) system in aqueous solution at four different temperatures (25, 45, 70, 100 °C) based on the stepwise equilibrium constants (Table 2) calculated from the NMR spectral integrals at each temperature. For each species the curves corresponding to the limiting temperatures of 25 and 100 °C are labeled; the temperature increase from one curve to the next follows the direction of the arrows. The black vertical line, corresponding to [Co] = 1×10^{-2} M, is to facilitate comparison with the ^{1}H NMR spectra in Figure 7; the ○ symbols show the intersection with the 25 °C curves, and the × symbols show the intersection with the 100 °C curves (see main text).

the speciation diagrams is limited by uncertainty in measurements of integral values of weak signals in paramagnetic complexes—in the $6\mathbf{Co_2} \rightleftharpoons \mathbf{Co_{12}}$ equilibrium constant, for example, the equilibrium constant includes an intensity measurement with an estimated uncertainty of ±20% raised to the sixth power—but the general behavior is clear.

As the temperature increases we see the curves that describe the proportions of each species at that temperature shift to the right such that the concentration at which $\mathbf{Co_{12}}$ disappears, and the smaller complexes appear, increases. Thus, at higher temperatures, a given concentration results in more fragmentation. The black line in Figure 11 drawn at [Co] = 1×10^{-2} M corresponds to the concentration used for the ^{1}H NMR spectra in Figure 7. From the intersections of this line with the 25 °C curves (marked by circles on Figure 11) we can see that the equilibrium solution contains $\mathbf{Co_{12}}$ as the major component, $\mathbf{Co_4}$ as a significant minor component, and almost no $\mathbf{Co_2}$, which agrees with the RT spectrum in Figure 7. Conversely the intersections of the black line with the 100 °C speciation curves (marked by crosses) show that the equilibrium solution is dominated by $\mathbf{Co_2}$ with a small amount of $\mathbf{Co_4}$ and virtually no $\mathbf{Co_{12}}$, which again agrees well with the 100 °C spectrum (top of Figure 7). The match between the observed ^{1}H NMR spectra in Figure 10, recorded at the higher concentration of [Co] = 0.1 M, and the calculated speciation behavior in Figure 11, is less quantitatively convincing—presumably because our model does not take into account the formation of the additional fourth species, larger than $\mathbf{Co_{12}}$, which starts to appear at high concentrations (purple circles in Figure 10).

We note also that Figure 11 shows how fortunate we were to be able to isolate crystals of $\mathbf{Co_4}$ from cold aqueous solution: the high concentrations (molar) in developing crystals should give almost exclusively $\mathbf{Co_{12}}$ under those conditions, except that the interconversion from $\mathbf{Co_4}$ to $\mathbf{Co_{12}}$ was clearly very slow at that temperature compared to the time scale of crystal growth (days).

CONCLUSIONS

The three complexes $[Co_2(L^{18w})_3]^{4+}$ ($\mathbf{Co_2}$, a dinuclear mesocate), $[Co_4(L^{18w})_6]^{8+}$ ($\mathbf{Co_4}$, a tetrahedral cage), and $[Co_{12}(L^{18w})_{18}]^{24+}$ ($\mathbf{Co_{12}}$, a truncated tetrahedral cage) exist in slow equilibrium with each other in aqueous solution. All three could be crystallized under different conditions and have been structurally characterized: in $\mathbf{Co_2}$ all three bridging ligands span both metal ions, whereas $\mathbf{Co_4}$ and $\mathbf{Co_{12}}$ are cages with a metal ion at each vertex and a bridging ligand spanning every edge. The equilibrium depends on both temperature and concentration and could readily be followed by ^{1}H NMR spectroscopy of the paramagnetic complexes. Increasing temperature and increasing dilution both favor fragmentation to give a large proportion of the smaller assemblies, for entropic reasons. In opposition to this, the hydrophobic effect favors reorganization of the smaller complexes to give $\mathbf{Co_{12}}$, which results in a greater proportion of the hydrophobic surface area being shielded from the water, so that the larger assembly dominates at high concentrations and low temperatures. Confirmation of this hypothesis comes from measurement of the product distribution in a nonaqueous solvent: in $MeNO_2$ (in which the complexes are sparingly soluble) only the smallest complex $\mathbf{Co_2}$ could be detected by ^{1}H NMR spectroscopy and mass spectrometry with no traces of the larger assemblies, whereas in water at the same low concentration, substantial proportions of $\mathbf{Co_4}$ are present. Thus, we have demonstrated a complex equilibrium between three structurally characterized metal–ligand assemblies, which can be understood on the basis of changes in temperature, concentration, and solvent, and we have calculated the speciation behavior for the $\mathbf{Co_2}/\mathbf{Co_4}/\mathbf{Co_{12}}$ system in water.

EXPERIMENTAL SECTION

General Details. Instrumentation used for ^{1}H NMR and low-resolution mass spectrometry measurements was described previously.[12] Ligand precursor **A** (Scheme 1) was prepared according to the published method.[12a] Other metal salts and organic reagents were obtained from Sigma-Aldrich and used as received. High-resolution mass spectra (see Supporting Information) were measured using a ThermoFisher Orbitrap Elite instrument equipped with an HESI source: full details of instrument settings and conditions are in Supporting Information.

Ligand Synthesis. *(i). Protected Ligand* ***B****.* A mixture of compound **A** (0.50 g, 1.73 mmol) and sodium hydride (60% dispersion in mineral oil; 0.069 g, 1.73 mmol) in dry tetrahydrofuran (THF, 25 cm^3) under N_2 was stirred for 10 min. 1,8-Bis-(bromomethyl)naphthalene (0.27 g, 0.86 mmol) was then added, and the mixture was stirred at 70 °C for 8 h, at which point an additional portion of sodium hydride (60% dispersion in mineral oil; 0.069 g, 1.73 mmol) was added. The reaction was monitored by thin layer chromatography (silica, CH_2Cl_2/MeOH, 95:5 v/v) until starting materials were consumed (~24 h). The reaction was then cooled to room temperature, and MeOH (10 cm^3) was added slowly and dropwise to destroy residual NaH. After evaporation of solvents the crude product was purified by column chromatography (silica, CH_2Cl_2/MeOH, 95:5 v/v). Traces of residual 1,8-bis(bromomethyl)-naphthalene elute with the solvent front; the product has an R_f of ~0.6, and other impurities adhered to the top of the column. Pure **B** was obtained as a yellow oil. Yield: 0.61 g, 97%. ES MS: m/z 731.4 $(M + H)^+$. ^{1}H NMR (400 MHz, $CDCl_3$): δ 0.13 (12H, s; Me), 0.96 (18H,

DOI: 10.1021/ic502780b
Inorg. Chem. 2015, 54, 2626–2637

s; ^{t}Bu), 4.79 (4H, s; CH_2O), 5.95 (4H, s; CH_2), 6.89 (2H, d, J = 2.5 Hz; pyrazolyl), 7.17 (2H, d, J = 2.5 Hz; pyrazolyl), 7.26 [4H, m; overlapping pyridyl H^5 and naphthyl ($H^{2/7}$ or $H^{4/5}$)], 7.48 (2H, t, J = 8.0 Hz; naphthyl $H^{3/6}$), 7.88 (2H, s; pyridyl H^3), 7.94 [2H, d, J = 8.0 Hz; naphthyl ($H^{2/7}$ or $H^{4/5}$)], 8.60 (1H, d, J = 5.0 Hz; pyridyl H^6).

(ii). Deprotected Ligand L^{18w}. To a solution of protected ligand **B** (0.610 g, 0.834 mmol) in THF (30 cm^3) was added tetrabutylammonium fluoride (0.530 g, 1.67 mmol); the reaction mixture was stirred for 18 h at room temperature. After this time $CHCl_3$ (40 cm^3) was added, and the mixture was stirred for a further 5 min. The mixture was then washed with water (3 × 50 cm^3); the remaining organic phase was dried over $MgSO_4$, and the solvent was removed to give a yellow solid. This was purified by column chromatography (silica, CH_2Cl_2/MeOH, 9:1 v/v) to afford pure L^{18w} as a white solid: in this case trace impurities elute first, and the polar ligand is the last fraction to elute with an R_f of ∼0.1. Yield: 0.41 g (96%). Low-resolution ESMS: m/z 503.2 $(M + H)^+$. High-resolution ESMS: observed, m/z 503.2173; $C_{30}H_{27}N_6O_2$ (MH^+) requires 503.2195. ^{1}H NMR (400 MHz, deuterated dimethyl sulfoxide (DMSO-d_6)): δ 4.53 (4H, d, J = 5.6 Hz; $C\underline{H}_2OH$—simplifies to singlet on D_2O shake), 5.46 (2H, t, J = 5.6 Hz; OH—disappears on D_2O shake), 6.22 (4H, s; CH_2), 6.91 (2H, d, J = 2.5 Hz; pyrazolyl), 7.02 (2H, d, J = 8.0 Hz; naphthyl $H^{2/7}$ or $H^{4/5}$), 7.23 (2H, d, J = 5.0 Hz; pyridyl H^5), 7.47 (2H, t, J = 8.0 Hz; naphthyl $H^{3/6}$), 7.73 (2H, d, J = 2.5 Hz; pyrazolyl), 7.90 (2H, s; pyridyl H^3), 7.97 (2H, d, J = 8.0 Hz; naphthyl $H^{2/7}$ or $H^{4/5}$), 8.47 (2H, d, J = 5.0 Hz; pyridyl H^6). Found: C, 62.3; H, 5.6; N, 14.4%. Required for $C_{30}H_{26}N_6O_2{\cdot}4H_2O$: C, 62.7; H, 6.0; N, 14.6%.

Syntheses of Complexes. A mixture of L^{18w} (30 mg, 0.06 mmol) and either $Co(ClO_4)_2{\cdot}6H_2O$ (14.6 mg, 0.04 mmol) or $Co(BF_4)_2{\cdot}6H_2O$ (13.6 mg, 0.04 mmol) in MeOH (8 cm^3) in a sealed Teflon-lined autoclave (total volume ca. 20 cm^3) was heated to 100 °C for 12 h in an oven and then slowly cooled (0.1 °C/min) to room temperature. The resulting orange solution was a mixture of the three complexes **Co_2**, **Co_4**, and **Co_{12}**. The complexes could be isolated as either their $[BF_4]^-$ or $[ClO_4]^-$ salts; however, X-ray quality crystals of **Co_2** and **Co_{12}** were best obtained as their $[BF_4]^-$ salts, and X-ray quality crystals of **Co_4** could only be obtained as the $[ClO_4]^-$ salt. ***Caution!*** *Perchlorate salts are potentially explosive, should only be prepared and handled in small quantities, and not subjected to mechanical shock or grinding.*

The conditions necessary for growing X-ray quality crystals of each component separately are as follows. Crystals of $[Co_2(L^{18w})_3](BF_4)_4$ (orange plates) were obtained by diffusion of diethyl ether or diisopropyl ether vapor into a solution of the crude product in $MeNO_2$. The yield of these from the crystallization was quantitative as the larger complexes do not form in this solvent (see main text). Crystals of $[Co_4(L^{18w})_6](ClO_4)_8$ (light orange blocks) were obtained in low yield from slow cooling of a solution of the crude reaction mixture in D_2O in an NMR tube. The crystallization was not allowed to go to completion to avoid contamination with crystals of **Co_{12}**, which also grow from aqueous solution. Crystals of $[Co_{12}(L^{18w})_{18}](BF_4)_{24}$ (orange blocks) were obtained in low yield from slow cooling of a solution of $[Co_{12}(L^{18w})_{18}](BF_4)_{24}$ that had been prepurified by size-exclusion chromatography on Sephadex G-50 column (see main text). Again the crystallization was not allowed to go to completion to avoid contamination with crystals of **Co_4**, which also grow from aqueous solution. ES mass spectra and ^{1}H NMR spectra were obtained on samples prepared using freshly redissolved crystals of the purified complexes.

Data for $[Co_2(L^{18w})_3](ClO_4)_4$: m/z 1923, 912, 575, 406 for $\{Co_2(L^{18w})_3(ClO_4)_{4-n}\}^{n+}$ (n = 1, 2, 3, 4, respectively). Accurate mass measurement for the signal from $\{Co_2(L^{18w})_3(ClO_4)_2\}^{2+}$: measured, m/z 911.1998; calculated for $C_{90}H_{78}N_{18}O_{14}Cl_2Co_2$, m/z 911.1993 (see Supporting Information).

Data for $[Co_4(L^{18w})_6](ClO_4)_8$: m/z 1926, 1251, 913 for $\{Co_4(L^{18w})_6(ClO_4)_{8-n}\}^{n+}$ (n = 2, 3, 4, respectively). Accurate mass measurements were performed on the tetrafluoroborate salt. For the signal from $\{Co_4(L^{18w})_6(BF_4)_5\}^{3+}$: measured, m/z 1228.3425; calculated for $C_{180}H_{156}N_{36}O_{12}B_5F_{20}Co_4$, m/z 1228.3448 (see Supporting Information).

Data for $[Co_{12}(L^{18w})_{18}](BF_4)_{24}$: m/z 1887, 1611, 1394, 1229, 1098, 990, 900 for $\{Co_{12}(L^{18w})_{18}(BF_4)_{24-n}\}^{n+}$ (n = 6, 7, 8, 9, 10, 11, 12, respectively). Accurate mass measurement for the signal from $\{Co_{12}(L^{18w})_{18}(BF_4)_{16}\}^{8+}$: measured, m/z 1392.7642; calculated for $C_{570}H_{494}N_{114}O_{38}B_{16}F_{64}Co_{12}$, m/z 1392.7638 (see Supporting Information).

Crystallography. The work to obtain the crystal structure of the ligand $L^{18w}{\cdot}HBF_4{\cdot}2CHCl_3$ was performed at the University of Sheffield using a Bruker Apex-2 diffractometer with a Mo Kα sealed tube source; data collection, solution, and refinement were routine, and the structure is shown in the Supporting Information.

For $[Co_2(L^{18w})_3](BF_4)_4$, $[Co_4(L^{18w})_6](ClO_4)_8{\cdot}18H_2O$, and $[Co_{12}(L^{18w})_{18}](BF_4)_{24}{\cdot}1.5H_2O$, data collections in each case were performed at the EPSRC National Crystallography Service at the University of Southampton, U.K., using a Rigaku FR-E+ diffractometer equipped with a Saturn 724+ CCD detector, using high-intensity Mo Kα radiation from either a rotating anode or a microfocus sealed-tube source.[21] Structure solution and refinement was with the SHELX suite of programmes.[22] In all cases crystals exhibited the usual problems of this type of structure, namely, weak scattering due to a combination of poor crystallinity, extensive solvation, and disorder of anions/solvent molecules. In each case the basic structure and connectivity of the complex cation could be unambiguously determined, which is all that is required for the purposes of this work. Extensive use of geometric restraints on aromatic rings, anions, and aromatic displacement parameters were required to keep refinements stable. Solvent molecules that could be modeled satisfactorily were included in the final refinements; in all cases large regions of diffuse electron density that could not be modeled (from disordered solvents/counterions) were removed from the refinement, using either the SQUEEZE function in PLATON (for **Co_4**)[23] or the "Solvent Mask" function in OLEX-2 (for **Co_2** and **Co_{12}**).[24] Full details are in the individual CIFs.

We emphasize that the compositions given in Table 1 are approximate not just because of severe disorder of anions/solvents but because the number of anions may be lower than expected (i.e., less than two per Co^{2+} ion) if some of the OH groups on the complex cations are deprotonated in the crystals: the high positive charge on the complex cations renders the OH groups acidic in aqueous solution, which makes this plausible.[18g] For **Co_2** the total electron count removed by the "solvent mask" in OLEX was 551 e/unit cell, which amounts to ca. 46 electrons per dinuclear complex unit. Only one and one-half of the expected four $[BF_4]^-$ anions could be located per dinuclear complex cation. The 46 e/complex unit removed during the refinement by the "solvent mask" function is equivalent to ca. one additional $[BF_4]^-$ anion, implying partial deprotonation of peripheral OH groups on the complex cation and therefore fewer anions than expected.

For **Co_4** the total electron count per unit cell removed by the "SQUEEZE" function in PLATON was 133 e, which amounts to ca. 33 electrons per tetranuclear complex unit. We could only locate seven $[ClO_4]^-$ anions per complex unit rather than the expected eight. The "SQUEEZED" electron density is insufficient to account for this missing anion (49 e) so we suggest that there are only seven $[ClO_4]^-$ anions per complex cation in the crystal due to loss of one acidic proton from the cation, with the 33 e/complex being equivalent to ca. three water molecules per complex.

For **Co_{12}** only four of the expected 24 $[BF_4]^-$ anions could be located per **Co_{12}** cation. The total electron count per unit cell removed by the "solvent mask" in OLEX was 3943 e/unit cell, or ca. 657 e/**Co_{12}** complex unit, which is consistent with ca. 16 $[BF_4]^-$ anions, giving a (maximum) total of 20 anions, or fewer anions plus solvent molecules. This is again consistent with partial deprotonation of OH groups during crystallization to reduce the high positive charge of the cage.

■ ASSOCIATED CONTENT

Ⓢ Supporting Information

Structural drawings of protonated ligand cation and complex cations, illustrations indicating geometric features of a complex cation and the situation of anions in the triangular and

DOI: 10.1021/ic502780b
Inorg. Chem. 2015, 54, 2626−2637

hexagonal faces of a complex cation, CIF files containing X-ray crystallographic data and structures. This material is available free of charge via the Internet at http://pubs.acs.org.

AUTHOR INFORMATION

Corresponding Author

*E-mail: m.d.ward@sheffield.ac.uk.

Notes

The authors declare no competing financial interest.

ACKNOWLEDGMENTS

We thank the EPSRC for a Ph.D. studentship (to W.C.), Dr. A Stephenson and Mr. H. Adams for assistance with the X-ray crystallography, and Dr. R. Beniston for recording the high-resolution mass spectra. Mass spectrometry analysis was undertaken in biOMICS, the University of Sheffield Faculty of Science Mass Spectrometry Facility, supported by funding from Yorkshire Cancer Research (SHEND01), the European Structural Fund Programme, and the University of Sheffield Alumni Fund.

REFERENCES

(1) Reviews on coordination cages: (a) Fiedler, D.; Leung, D. H.; Bergman, R. G.; Raymond, K. N. *Acc. Chem. Res.* **2005**, *38*, 349. (b) Fujita, M.; Tominaga, M.; Hori, A.; Therrien, B. *Acc. Chem. Res.* **2005**, *38*, 369. (c) Seidel, S. R.; Stang, P. J. *Acc. Chem. Res.* **2002**, *35*, 972. (d) Hamilton, T. D.; MacGillivray, L. R. *Cryst. Growth Des.* **2004**, *4*, 419. (e) Ward, M. D. *Chem. Commun.* **2009**, 4487. (f) Perry, J. J.; Perman, J. A.; Zaworotko, M. J. *Chem. Soc. Rev.* **2009**, *38*, 1400. (g) Alvarez, S. *Dalton Trans.* **2006**, 2209. (h) Amouri, H.; Desmarets, C.; Moussa, J. *Chem. Rev.* **2012**, *112*, 2015. (i) Williams, A. F. *Coord. Chem. Rev.* **2011**, *255*, 2104. (j) Laughrey, Z.; Gibb, B. *Chem. Soc. Rev.* **2011**, *40*, 363. (k) Jin, P.; Dalgarno, S. J.; Atwood, J. L. *Coord. Chem. Rev.* **2012**, *254*, 1760. (l) Chakrabarty, R. J.; Mukherjee, P. S.; Stang, P. J. *Chem. Rev.* **2011**, *111*, 6810. (m) Inokuma, Y.; Kawano, M.; Fujita, M. *Nat. Chem.* **2011**, *3*, 349. (n) Pluth, M. D.; Bergman, R. G.; Raymond, K. N. *Acc. Chem. Res.* **2009**, *42*, 1650. (o) Breiner, B.; Clegg, J. K.; Nitschke, J. R. *Chem. Sci.* **2011**, *2*, 51. (p) Smulders, M. M. J.; Riddell, I. A.; Browne, C.; Nitschke, J. R. *Chem. Soc. Rev.* **2013**, *42*, 1728. (q) Nakamura, T.; Ube, H.; Shionoya, M. *Chem. Lett.* **2014**, *42*, 328.

(2) (a) Saalfrank, R. W.; Stark, A.; Peters, K.; von Schnering, H. G. *Angew. Chem., Int. Ed. Engl.* **1988**, *27*, 851. (b) Saalfrank, R. W.; Stark, A.; Bremer, M.; Hummel, H.-U. *Angew. Chem., Int. Ed. Engl.* **1990**, *29*, 311.

(3) (a) Tominaga, M.; Suzuki, K.; Kawano, M.; Kusukawa, T.; Ozeki, T.; Sakamoto, S.; Yamaguchi, K.; Fujita, M. *Angew. Chem., Int. Ed.* **2004**, *43*, 5621. (b) Sun, Q.-F.; Iwasa, J.; Ogawa, D.; Ishido, Y.; Sato, S.; Ozeki, T.; Sei, Y.; Yamaguchi, K.; Fujita, M. *Science* **2010**, *328*, 1144. (c) Harris, K.; Fujita, D.; Fujita, M. *Chem. Commun.* **2013**, *49*, 6703.

(4) Ward, M. D.; Raithby, P. R. *Chem. Soc. Rev.* **2013**, *42*, 1619.

(5) Northrop, B. H.; Zheng, Y.-R.; Chi, K.-W.; Stang, P. J. *Acc. Chem. Res.* **2009**, *42*, 1554.

(6) (a) Clever, G. H.; Kawamura, W.; Tashiro, S.; Shiro, M.; Shionoya, M. *Angew. Chem., Int. Ed. Engl.* **2012**, *51*, 2606. (b) Han, M.; Hey, J.; Kawamura, W.; Stalke, D.; Shionoya, M. *Inorg. Chem.* **2012**, *51*, 9574. (c) Clever, G. H.; Tashiro, S.; Shionoya, M. *J. Am. Chem. Soc.* **2010**, *132*, 9973.

(7) (a) Stephenson, A.; Argent, S. P.; Riis-Johannessen, T.; Tidmarsh, I. S.; Ward, M. D. *J. Am. Chem. Soc.* **2011**, *133*, 858. (b) Albrecht, M.; Janser, I.; Runsink, J.; Raabe, G.; Weis, P.; Fröhlich, R. *Angew. Chem., Int. Ed.* **2004**, *43*, 6662. (c) Cotton, F. A.; Murillo, C. A.; Yu, R. *Dalton Trans.* **2006**, 3900. (d) Yamanoi, Y.; Sakamoto, Y.; Kusukawa, T.; Fujita, M.; Sakamoto, S.; Yamaguchi, K. *J. Am. Chem. Soc.* **2001**, *123*, 980. (e) Umemoto, K.; Yamaguchi, K.; Fujita, M. *J. Am. Chem. Soc.* **2000**, *122*, 7150. (f) Fujita, M.; Sasaki, O.; Mitsuhashi, T.; Fujita, T.; Yazaki, J.; Yamaguchi, K.; Ogura, K. *Chem. Commun.* **1996**, 1535. (g) Chand, D. K.; Biradha, K.; Kawano, M.; Sakamoto, S.; Yamaguchi, K.; Fujita, M. *Chem.—Asian J.* **2006**, *1*−*2*, 82. (g) Samanta, D.; Mukherjee, P. A. *Chem.—Eur. J.* **2014**, *20*, 12483. (h) Meng, W.; Ronson, T. K.; Clegg, J. K.; Nitschke, J. R. *Angew. Chem., Int. Ed.* **2013**, *52*, 1017. (i) Riddell, I. A.; Hristova, Y. R.; Clegg, J. K.; Wood, C. S.; Breiner, B.; Nitschke, J. R. *J. Am. Chem. Soc.* **2013**, *135*, 2723. (j) Scherer, M.; Caulder, D. L.; Johnson, D. W.; Raymond, K. N. *Angew. Chem., Int. Ed. Engl.* **1999**, *38*, 1588. (k) Chen, Q.; Jiang, F.; Yuan, D.; Lyu, G.; Chen, L.; Hong, M. *Chem. Sci.* **2014**, *5*, 483.

(8) (a) Lehn, J.-M. *Chem.—Eur. J.* **1999**, *5*, 2455. (b) Cougnon, F. B. L.; Sanders, J. K. M. *Acc. Chem. Res.* **2012**, *45*, 2211. (c) Moulin, E.; Cormos, G.; Guiseppone, N. *Chem. Soc. Rev.* **2012**, *41*, 1031.

(9) (a) Campos-Fernandez, C. S.; Schottel, B. L.; Chifotides, H. T.; Bera, J. K.; Bacsa, J.; Koomen, J. M.; Russell, D. H.; Dunbar, K. R. *J. Am. Chem. Soc.* **2005**, *127*, 12909. (b) Hasenknopf, B.; Lehn, J.-M.; Boumediene, N.; Dupont-Gervais, A.; Van Dorsselaer, A.; Kneisel, B.; Fenske, D. *J. Am. Chem. Soc.* **1997**, *119*, 10956.

(10) Baxter, P. N. W.; Lehn, J.-M.; Baum, G.; Fenske, D. *Chem.—Eur. J.* **2000**, *6*, 4510.

(11) (a) Argent, S. P.; Adams, H.; Riis-Johannessen, T.; Jeffery, J. C.; Harding, L. P.; Mamula, O.; Ward, M. D. *Inorg. Chem.* **2006**, *45*, 3905. (b) Bell, Z. R.; Jeffery, J. C.; McCleverty, J. A.; Ward, M. D. *Angew. Chem., Int. Ed.* **2002**, *41*, 2515.

(12) (a) Whitehead, M.; Turega, S.; Stephenson, A.; Hunter, C. A.; Ward, M. D. *Chem. Sci.* **2013**, *4*, 2744. (b) Turega, S.; Cullen, W.; Whitehead, M.; Hunter, C. A.; Ward, M. D. *J. Am. Chem. Soc.* **2014**, *136*, 8475. (c) Cullen, W.; Turega, S.; Hunter, C. A.; Ward, M. D. *Chem. Sci.* **2015**, *6*, 625.

(13) (a) Amouri, H.; Mimassi, L.; Rager, M. N.; Mann, B. E.; Guyard-Duhayon, C.; Raehm, L. *Angew. Chem., Int. Ed.* **2005**, *44*, 4543. (b) Tidmarsh, I. S.; Taylor, B. F.; Hardie, M. J.; Russo, L.; Clegg, W.; Ward, M. D. *New J. Chem.* **2009**, *33*, 366. (c) Hall, B. R.; Manck, L. E.; Tidmarsh, I. S.; Stephenson, A.; Taylor, B. F.; Blaikie, E. J.; Vander Griend, D. A.; Ward, M. D. *Dalton Trans.* **2011**, *40*, 12132. (d) Turega, S.; Whitehead, M.; Hall, B. R.; Meijer, A. J. H. M.; Hunter, C. A.; Ward, M. D. *Inorg. Chem.* **2013**, *52*, 1122.

(14) (a) Albrecht, M.; Kotila, S. *Angew. Chem., Int. Ed.* **1995**, *34*, 2134. (b) Xu, J.; Parac, T. N.; Raymond, K. N. *Angew. Chem., Int. Ed.* **1999**, *38*, 2878. (c) Zhang, Z.; Dolphin, D. *Chem. Commun.* **2009**, 6931. (d) Ronson, T. K.; Adams, H.; Riis-Johannessen, T.; Jeffery, J. C.; Ward, M. D. *New J. Chem.* **2006**, *30*, 26.

(15) (a) Harding, L. P.; Jeffery, J. C.; Riis-Joannessen, T.; Rice, C. R.; Zeng, Z. T. *Dalton Trans.* **2004**, 2396. (b) Albrecht, M.; Fröhlich, R. *J. Am. Chem. Soc.* **1997**, *119*, 1656.

(16) (a) Fleming, J. S.; Mann, K. L. V.; Carraz, C.-A.; Psillakis, E.; Jeffery, J. C.; McCleverty, J. A.; Ward, M. D. *Angew. Chem., Int. Ed.* **1998**, *37*, 1279. (b) Paul, R. L.; Bell, Z. R.; Jeffery, J. C.; McCleverty, J. A.; Ward, M. D. *Proc. Natl. Acad. Sci. U. S. A.* **2002**, *99*, 4883.

(17) Cotton, F. A.; Murillo, C. A.; Yu, R. *Dalton Trans.* **2005**, 3161.

(18) (a) Southall, N. T.; Dill, K. A.; Haymet, A. D. J. *J. Phys. Chem. B* **2002**, *106*, 521. (b) Hummer, G.; Garde, S.; García, A. E.; Paulaitis, M. E.; Pratt, L. R. *J. Phys. Chem. B* **1998**, *102*, 10469. (c) Pratt, L. R.; Pohorille, A. *Chem. Rev.* **2001**, *102*, 2671. (d) Tanford, C. *Science* **1978**, *200*, 1012. (e) Houk, K. N.; Leach, A. G.; Kim, S. P.; Zhang, X. *Angew. Chem., Int. Ed.* **2003**, *42*, 4872. (f) Meyer, E. A.; Castellano, R. K.; Diederich, F. *Angew. Chem., Int. Ed.* **2003**, *42*, 1210. (g) Hunter, C. A. *Chem. Sci.* **2013**, *4*, 834.

(19) We showed recently that burial of an aromatic ring in the hydrophobic cavity of a cage from this family resulted in stabilisation by 0.12 kJ mol^{-1} per $Å^2$ of desolvated surface (ref 12a). On this basis combining three $\mathbf{Co_4}$ complexes into a single $\mathbf{Co_{12}}$ complex in aqueous solution would afford ~160 kJ mol^{-1} of stabilization from the hydrophobic effect. This must be substantially offset by factors favouring fragmentation into smaller assemblies, or the smaller assemblies would never form, but it gives an indication of the magnitude of the effect. In fact from ^{1}H NMR integrals we can

DOI: 10.1021/ic502780b
Inorg. Chem. 2015, 54, 2626−2637

estimate the $3\mathbf{Co_4} \rightleftharpoons \mathbf{Co_{12}}$ equilibrium constant, which gives $\Delta G^\circ = -41$ kJ mol^{-1} at 298 K (section viii, Table 2).
(20) Stephenson, A.; Sykes, D.; Ward, M. D. *Dalton Trans.* **2013**, *42*, 6756.
(21) Coles, S. J.; Gale, P. A. *Chem. Sci.* **2012**, *3*, 683.
(22) Sheldrick, G. M. *Acta Crystallogr., Sect. A* **2008**, *64*, 112.
(23) (a) Spek, A. L. *J. Appl. Crystallogr.* **2003**, *36*, 7. (b) van der Sluis, P.; Spek, A. L. *Acta Crystallogr., Sect. A: Found. Crystallogr.* **1990**, *46*, 194.
(24) Dolomanov, O. V.; Bourhis, L. J.; Gildea, R. J.; Howard, J. A. K.; Puschmann, H. *J. Appl. Crystallogr.* **2009**, *42*, 339.

DOI: 10.1021/ic502780b
Inorg. Chem. 2015, 54, 2626−2637